Mitigation of impact of a major benzene spill into a river through flow control and in-situ activated carbon absorption

Guangqiu Jin[a], Zhongtian Zhang[a], Yihang Yang[b], Shuheng Hu[a], Hongwu Tang[a,*], David Andrew Barry[c], Ling Li[d,*]

[a] State Key Laboratory of Hydrology-Water Resources and Hydraulic Engineering, Hohai University, Nanjing, China

Emails: jingq@hhu.edu.cn, zhongtian_zhang@163.com, shuheng_hu@126.com, hwtang@hhu.edu.cn,

[b] China Water Huaihe Planning, Design and Research Co., Ltd, Hefei, China

Email: pedro_hang@outlook.com

[c] Laboratoire de technologie écologique, Institut d'ingénierie de l'environnement, Faculté de l'environnement naturel, architectural et construit (ENAC), Ecole Polytechnique Fédérale de Lausanne (EPFL), Station 2, 1015 Lausanne, Switzerland

Email: andrew.barry@epfl.ch

[d] School of Engineering, Westlake University, Hangzhou, China

Email: liling@westlake.edu.cn

Resubmitted to *Water Research* on 19 November 2019

* Authors to whom all correspondence should be addressed. Emails: hwtang@hhu.edu.cn; liling@westlake.edu.cn

Abstract

Benzene is a toxic contaminant and can harm many aquatic species and cause serious damages to the river eco-system, if released to rivers. In 2012, a major spill accident occurred on the Huaihe River in Eastern China with 3 tons of benzene released to the river section 70 km upstream of a natural reserve. Two emergency measures were taken to minimize the impact of the accident on the natural reserve: 1) flow control by adjusting upstream sluices to delay the arrival of the contaminant plume at the reserve and 2) in-situ treatment using activated carbons to reduce the contaminant concentration. Here we develop a process-based mathematical model to analyze the monitoring data collected shortly after the accident, and explore not only how effective the adopted measures were over the incident but more importantly the mechanisms and critical conditions underlying the effectiveness of these measures. The model can be used as a tool for designing optimal management responses to similar spill accidents in regulated river systems, combining flow control and in-situ treatment.

Keywords: Huaihe River; Benzene pollution; Accidental contaminant release; Flow adjustment; Activated carbons

1 Introduction

Pollution incidents, involving accidental release of contaminants to the environment, happen around the world. Between 2001 and 2007, about 700 major water pollution incidents each year were recorded in China (Ji et al., 2017). From 2001 to 2016, about 470 major water pollution incidents in total took place in the UK (Tiseo, 2018), while about 120 water pollution incidents over main river reaches were registered in Japan from 1996 to 2007 (Duan et al., 2013). Indeed water pollution incidents are a major issue in many countries around the world. During these incidents, toxic contaminants may be discharged into rivers, causing serious damages on the aquatic ecosystem (Palumbo-Roe et al., 2017; Mandaric et al., 2019). In 2012, three tons of

benzene was suddenly released into a major river in Eastern China, the Huaihe River, due to an industrial accident on 28th December at a location 3.5 km downstream of the Bengbu Sluice on the river and around 70 km upstream of a natural reserve. The benzene plume travelled downstream and presented a threat to the natural reserve. The concentration of benzene in the river water must be maintained at a level below the regulatory limit (0.01 mg/L) required for the protection of the reserve when the plume passed through. The local government and river regulation agency took an immediate emergency action to reduce the benzene concentration, combining flow control and in-site treatment with activated carbon (AC). The Bengbu Sluice was adjusted to lower the river discharge from 150 m^3/s to 25 m^3/s and around 150 tons of AC was put into the river at three locations downstream of the benzene release point.

Previous studies indicated that benzene can be absorbed by different types of particles (Majumder et al., 2003; Zhao and Ward, 1999). Activated carbon particles with large surface areas were put into the river to remove benzene from the river water after the accident on the Huaihe River. While this treatment produced the benefit of reducing the benzene concentration in the river water, the carbon particles with absorbed benzene would settle down and even enter the bed with hyporheic exchange flow, potentially affecting the hyporheic zone eco-system (Roy et al., 2018; Bjerg et al., 2017). Moreover, the absorbed benzene may later be released back to the river water (Ren and Packman, 2005; Saup et al., 2017; Feijoó et al., 2018; Jin et al., 2018; Jin et al., 2019), causing secondary pollution. Combined with the activated carbon treatment, river sluices could be operated to reduce the river flow to allow more time for mixing and absorption of benzene before the plume reached critical locations downstream. On the Huaihe River, there are a relatively large number of sluices that can be operated for this purpose (Wang and Ongley, 2004; Zuo et al., 2015). This study focuses on determining the factors that influence the benzene transport and transformation process during the 2012 major pollution incident in the Huaihe River, evaluating the effects of different management measures (including discharge control and in-situ treatment using activated carbon), and developing tools

and strategies for similar incidents.

During the 2012 pollution incident, the Huaihe River Basin Water Resources Protection Bureau and Hohai University monitored the benzene concentrations in the river water at 22 given cross-sections downstream of the accident location (Fig. 1 and 2). While the data showed that the emergency response appeared to have successfully mitigated the impact of the accident on the river and natural reserve, the mechanism and critical conditions underlying the effectiveness of the measures taken require further investigation. In addition to absorption and mixing, the fate of benzene released to the Huaihe Rivers could be affected by volatilization and natural attenuation. By analyzing the monitoring data using a mathematical model, we aimed to learn further lessons from the Huaihe River incident by addressing the following questions: 1) which process/es among volatilization, naturally attenuation and AC-adsorption dominated the removal of benzene from the river water? 2) how do the flow control (via the sluice operation) and in-situ treatment (through active carbon adsorption) combine to reduce the benzene concentration to the required limit? and 3) how should an emergency pollution control strategy and management/engineering solution be formulated over a pollution incident on a regulated river in general?

2 Method

The benzene concentrations measured at the 22 cross-sections (P1 to P22, Fig. 1) are shown Fig. S1. To analyze the concentrations, a process-based mathematical model was developed. This model simulates the transport and transformation of benzene over the downstream river section from the Bengbu Sluice to the last monitoring location (P22; Fig. 1), and the flow-process is in Fig.3a. This river section was divided into ten segments (S1 to S10; Fig. 1), each of similar geomorphology (including the geometry of river cross-section) and vegetation. The geometries of representative cross-sections for the 10 segments were measured at H1 to H10, respectively (Fig. 1). For each segment, the Manning equation (e.g. Bjerklie et al., 2005) is used to determine the relationship among average flow rate (u m/s), discharge (Q m^3/s) and average

cross-section area (A m^2), i.e.,

$$u = \frac{1}{n_m} r^{2/3} J^{1/2} \tag{1}$$

$$Q = A \cdot u \tag{2}$$

$$r = \frac{A}{\chi} \tag{3}$$

where n_m is the bed roughness factor, J (m) is the river bed slope, r (m) is the hydraulic radius, and χ (m) is the wetted perimeter (Fig.2).

The transport and transformation of benzene through each segment within the modeled river section are governed by the 1-D transport-reaction equation (e.g. Wang et al., 2006; Fu et al., 2008),

$$\frac{\partial C}{\partial t} = -u \frac{\partial C}{\partial x} + D \frac{\partial^2 C}{\partial x^2} - KC \tag{4}$$

where C (kg/m^3) is the benzene concentration in the river water, t (s) is the time, x (m) is the distance from the accident point (upstream boundary of the whole river section), D (m^2/s) is the dispersion coefficient, and K (1/s) is the total attenuation coefficient. Three attenuation processes were considered: volatilization, AC adsorption and natural attenuation (with benzene converted to another chemical). Thus the total attenuation coefficient includes three parts,

$$K = k_{ac} + k_{na} + \lambda \tag{5}$$

where k_{ac} (1/s) is the adsorption coefficient of activated carbons, k_{na} (1/s) is the natural attenuation coefficient, and λ (1/s) is the volatilization coefficient. The volatilization coefficient can be determined as follows (Trapp et al., 1995),

$$\frac{1}{\lambda} = \left(\frac{1}{k_1} + \frac{1}{K_{AW} \cdot k_g} \right) \cdot h \tag{6}$$

where K_{AW} [-] is the partition coefficient between air and water from Henry's law; k_g (m/s) is the transfer velocity (conductivity) of the gas layer and can be determined as below,

$$k_g = 1.517 \times 10^{-3} \bullet (u + v_w) \tag{7}$$

where v_w (m/s) is the speed of wind at 10 cm above the water. k_1 (m/s) is the transfer velocity (conductivity) of the liquid layer, and can be determined by:

$$k_1 = 4.053 \times 10^{-5} \bullet uh^{-0.673} \bullet 1.022^{(Temp\text{-}20\ ^{\circ}\mathrm{C})} \tag{8}$$

where *Temp* (℃) is the temperature, *h* (m) is he average water depth. The average water depth (*h* m) can be calculated based on the cross-section geometry.

In order to derive the analytical solution, the model was developed based on the averaged flow rates (constant) during the incident for the purpose of simplicity. For the 1-D transport-reaction equation (4) with a sudden input, the analytical solution can be found below (e.g. Van Genuchten, 1982; Kumar et al., 2009),

$$C(x,t) = \frac{m / A_0}{\sqrt{4\pi Dt}} \exp\left(-\frac{(x-ut)^2}{4Dt} \right) \cdot \exp(-Kt) \tag{9}$$

where *m* (kg) is the sudden input mass, and A_0 (m^2) is the area of the cross-section at the input (x_0). However, this solution is only applicable for the first segment (S1), where the sudden benzene mass input occurred at the release point. For S2 to S10, the mass input boundary condition was given by the entry of the plume with temporally varying concentrations. As shown in Fig. 3b, given C (x_n, τ) as the input concentration at the upstream boundary (x_n) of the *n*-th segment, the benzene concentration varying along this segment can be obtained as follows,

$$C(x_{n+1} + d, t) = \frac{A_n}{A_{n+1}} \int_0^t \frac{u_{n+1} C(x_n, \tau)}{\sqrt{4\pi D_{n+1}(t-\tau)}} \exp\left(-\frac{[d - u_{n+1}(t-\tau)]^2}{4D_{n+1}(t-\tau)} \right) \cdot \exp[-K_{n+1}(t-\tau)]\, \mathrm{d}\tau \tag{10}$$

where u_n, D_n and K_n are the flow velocity, dispersion coefficient and total attenuation coefficient for segment *n*. *d* (variable) is the distance from the segment's upstream boundary (x_n) and in the range of [0, x_{n+1}-x_n] where x_{n+1} is the distance of the downstream boundary of segment *n* or upstream boundary of segment *n*+1 from the Bengbu Sluice. τ (s) is the time for the *n*-th process, while *t* (s) is the time for the (*n*+1)-th process. Note that equation (10) is applied progressively to the segments from S2 to S10, taking the output

from the current segment as the input to the next segment with the change of the cross-section area taken into account; so $C(x_{n+1},t)$ calculated by equation (10) should be corrected by a factor of A_n/A_{n+1} before using it as the input into segment n+1.

All the model parameters values are listed in Table 1. The values of slopes (J) and roughness (n_m) factors were based on previous studies (Beng, 2010; Wang et al., 2014). The relationships among average flow velocity (u m/s), average depth of water (h m), and average area (A m^2) were determined through the Manning equations (Eq.1, 2 & 3) with the measured geometries of the cross-sections and discharge (Q m/s^3). The results are shown in Fig.2c & d and Fig. S2. The volatilization coefficient was calculated by Eq. 6 based on the average flow velocity (u m/s) and average water depth (h m). The total attenuation coefficient (K 1/s) and dispersion coefficient (D m^2/s) were based on model calibration by fitting model predictions (Eqs. 9 and 10) to measured benzene concentration data (P1-P22). Nevertheless, we estimated the values of D with the following empirical formula (Fischer, 1975),

$$D = 0.011\, u^2 B^2 / (h u_*) \tag{11}$$

where B (m) is the width of the river, and u_* ($u_* = \sqrt{ghJ}$, m/s) is the friction velocity. The typical value range of D in the reach of Huaihe River we studied is 1.5 – 9.7 m^2/s (Deng et al., 2002), which covers the fitted value (Table 1).

3 Results and discussion

Four simulation cases were considered: Case A representing the real situation with flow control and activated carbons measures implemented, Case B with activated carbons applied but no flow control, Case C with flow control but no activated carbons applied and Case D without flow control or activated carbons applied.

3.1 Spatial and temporal variations of benzene concentrations in the river water

Measurements and model predictions (Case A) of benzene concentrations at all the monitoring

locations agree reasonably well, both showing similar trends with a rising and a falling phase at P2-P22 (Fig. 4 and S1). With no flow control (Case B), the model predicted earlier arrivals and larger magnitudes of peak concentrations at all the monitoring locations compared with Case A (Fig. 4 and S1). The arrival time of peak concentration in Case A lagged that in case B by 21.6 h at P6 and 54.2 h at P11 (Fig. 4). Another way to estimate the peak concentration time is based on the flow time, T_a, for a particular location (x) within segment n calculated as follows,

$$T_a = \begin{cases} \sum_{i=1}^{n-1} \frac{L_i}{u_i} + \frac{x - \sum_{i=1}^{n-1} L_i}{u_n} & (\text{if } n \geq 2) \\ \frac{x}{u_n} & (\text{if } n = 1) \end{cases} \tag{12}$$

where L_i is the length of the i-th segment. Equation (12) provides estimates of T_a being 64.0 h and 43.5 h for P6 and P11 in Case A, while the actual arrival times of peak concentration were 66.0h and 43.1 h, respectively. For Case B, T_a was 164.2 h for P6 and 108.9 h for P11; and the corresponding arrival times of peak concentration were 164.8 h and 110.6 h, respectively. The peak concentration was higher with larger flow rates in Case B than in Case A (Fig. 5), as the time for benzene mixing and attenuation became shorter in the former case. Similar effect was also evident in Case D in comparisons with case C. Comparisons between Case A and Case C, and Case B and Case D revealed the effect of active carbons, which led to reduction in the benzene concentrations, including the peak concentration but did not change the arrival time of peak concentrations (Fig. 4 and 5).

Overall, the peak concentration decreased from P1 to P22, as the benzene plume mixed with ambient water (dilution) and underwent attenuation (for case A and B) over distance and time (Fig. 6). In Case A and B, the peak concentrations also responded to the input of AC with an immediate drop (Fig. 6), demonstrating the strong AC adsorption effect on the removal of benzene from the river water. To further assess the local pollution, we calculated the duration over which the benzene concentration exceeds the regulatory limit as

the plume passed through a location (Fig. 7). In all cases, this duration (T_p) increased with distance initially, then remained relatively constant, and finally decreased dramatically (Fig. 7). The initial lengthening of the local pollution duration in upstream areas near the benzene release point was due to benzene dispersion, which dominated over the attenuation process and resulted in spreading of the plume of relatively high concentrations. The rapid shortening of the local pollution duration in the downstream areas reflected the significant attenuation of the plume over the distance, with the peak concentration close to and dropping quickly below the regulatory limit. In the middle reach, the effects of dispersion and attenuation balanced each other, keeping T_p relatively constant. Dramatic drops of T_p in the segments where activated carbons (AC) were put into the river were clearly evident as simulated in Case A and B. This again demonstrated the effect of AC adsorption on removing benzene from the river water. The comparisons among the four simulation cases showed how flow control and in-situ treatment using AC could be applied to mitigate the impact of a pollution accident/incident on a river system.

3.2 Fate of benzene with distributions in different phases

The reach of the Huaihe River where this study focus on is divided into 2 reaches: Reach A (RA) and Reach B (RB), and RA represents S1 while RB represents S2+S3+…+S10 (Fig. 1). This study is focus on RB, as the monitoring data in P3 is relative credible. The benzene in RA might be heterogeneous mixing. The removed benzene from the river water would be in the volatilized phase, transformed phase and AC-adsorbed phase. According to the model simulations, most of the mass was in the AC-absorbed phase (and likely to have settled on the river bed) and volatilized phase (Table 2). Under the real condition (Case A), only about 10% of the benzene mass was transformed, and around 42% and 48% were volatilized and AC-adsorbed, respectively (Table 2). In Case C and D with no input of AC, most of the benzene mass was volatilized (Table 2). Comparison between Case A and B (or Case C and D) indicated that a larger flow rate resulted in less volatilized mass (Table 2).

Both volatilized mass and transformed mass decreased with the distance (Fig. 8a). The AC adsorption occurred rapidly within the three sections with the AC input. To further analyze the benzene mass in different phases/forms, we calculated the mass per kilometer for each phase normalized by the total benzene mass, i.e., $M^* = M / m_{RB}$. M^* of the transformed benzene was almost the same in both Case A and Case B, while M^* of the volatilized in Case B was only half of that in Case A. The AC-adsorbed mass was very high in the three sections with AC input, since the AC adsorption coefficient is several times higher than the natural attenuation coefficient and volatilization coefficient (Table 1). Comparison between Case A and Case B showed that M^* of the AC-adsorbed benzene was higher in Case A than in Case B in the first segment of AC input because the faster flow in the latter case resulted in less time for benzene to be adsorbed. In the second segment, the two cases differed little. However, M^* in the last segment was lower in Case A than in Case B (Fig. 8a). In this segment, the benzene concentration in Case A was low, resulting in less adsorption.

The temporal variations of the benzene mass in different phases were also examined (Fig. 8b). The benzene mass in the water phase decreased continuously, in contrast with the increasing trends of the other phases. Rapid increase in the absorbed benzene mass occurred in Case A and Case B corresponding to the AC input (Fig. 8b), consistent with the spatial variations shown in Fig. 8a. There were 3 dramatic increases in the mass of AC-adsorbed benzene in Case A starting around 125 h, 175 h and 225 h when the AC was input to the river. Consequently, the water phase benzene mass dropped more rapidly around these times (Fig. 8b).

3.3 Effectiveness of pollution control options

Based on the model simulation results, the pollution zone bounded by the edges (x coordinates) of the benzene plume of concentrations above the regulatory limit can be determined at different times. Over the incident, the extents of the pollution zone simulated in the different cases can be assessed based on the edges curves shown in Fig. 9. These closed curves display how the spatial extent of the pollution zone changed

over time with a trend of expansion followed by contraction to non-existence (i.e., the front tip of the curve highlighted in the figure). At a particular location, the edges curves show the temporal extent of the pollution, indicating the passing-though period of the benzene plume above the regulatory limit. The front tips of these curves provide information about how far the pollution incident impacts on the downstream river reach with benzene concentrations above the regulatory limit and for how long. The spatial and temporal extents of the pollution zones simulated in the four different cases are consistent with the results discussed above.

The simulations show that in the actual event (Case A), the incident lasted for 312.5 h and affected the downstream area covering 58.2 km from the benzene release point but fortunately falling short of 17.2 km from the natural reserve (Table 3 & Fig. 9). The two implemented emergency measures were effective in reducing the pollution extent to avoid damage on the natural reserve. In Case B, C and D simulated with less or no measures undertaken, the incident would have caused damages (Case C and D) or presented a threat (Case B with the front tip being close the reserve) to the natural reserve (Table 3 & Fig. 9). Comparison between Case A and C indicates that the in-situ treatment with the input of AC reduced significantly both the spatial and temporal extents of benzene pollution, despite little effect on the movement of the peak concentration (i.e., most polluted section of the plume; Fig. 9). On the other hand, the difference between Case A and B shows again the effect of flow rates; in particular, under a larger flow rate, the pollution incident may last for a shorter duration but with the risk of causing pollution for a larger downstream area (Fig. 9).

3.4 Sensitivity analysis

To assess the sensitivity of the modelled benzene transport/transformation process to different conditions, we conducted further analyses based on different values of dispersion coefficient (D), flow rate (u) and adsorption coefficient of activated carbons (k_{ac}) with a focus on changes of pollution length (L_m), pollution duration (T_m) and peak concentration (C_m). The results of spatial and temporal range of pollution

are shown in Table 4 and Fig. 10. The concentration profiles are shown in Fig. 11, Fig. S3, Fig. S4 and Fig. S5. The peak concentration variations are shown in Fig. S6.

With the increase of flow velocity (u), the pollution length (L_m) increases but the pollution duration (T_m) decreases (Fig.10a & Table 4). The local contaminant concentration at a cross-section increases with the arrival time of peak concentration brought forward and the contamination duration shortened (Fig.11a,b, Fig.S3 and Fig.S6). As the larger flow rate leads to faster downstream movement of the contaminant, there is less time for the plume to spread, resulting in a more concentrated plume moving farther downstream.

In contrast, a larger dispersion coefficient (D) reduces the overall spatial and temporal extents of contamination (Fig.10b & Table 4). However, the spatial range of the pollution plume becomes larger at a particular time, while at a given location, the temporal range of the pollution plume becomes greater. The variation of dispersion coefficient does not affect the arrival time of peak concentration (Fig.10b & fig.11c,d).

Large adsorption coefficients of activated carbons (k_{ac}) also lead to smaller spatial and temporal benzene distributions (Fig.10c & Table 4). At a given time, the spatial range of the contaminant plume becomes narrower, while the temporal range of the pollution plume at a given location becomes shorter. The variation of the adsorption coefficient does not affect the arrival time of peak concentration either (Fig.10c & fig.11e,f).

In order to quantify the sensitivity of the benzene transport/transformation process in response to condition changes, all the parameters are normalized (Fig.12) by "real" values based on Case A. The pollution length, pollution duration, peak concentration, dispersion coefficient, flow rate and adsorption coefficient of activated carbons are normalized as L_m/L_{m0}, T_m/T_{m0}, C_m/C_{m0}, D/D_0, u/u_0, and k_{ac}/k_{ac0}, respectively.

Obviously, the effects of u on L_m and C_m are positive but negative for T_m (Fig.12a), reflecting that the

peak concentration and the spatial range of pollution increase with flow rate, but the temporal range of pollution decreases. The sensitivity of C_m to u at P11 is greater than at P6 (Fig.12a). This suggests that the influence of u on C_m is stronger at locations which is farther from the contaminant release point. The effects of D on T_m, L_m and C_m are negative. The sensitivity of C_m to D at two different locations are similar, and so are the sensitivity of T_m and L_m to D (Fig. 12b). The effects of k_{ac} on T_m, L_m and C_m are negative (Fig. 12c). The sensitivity of C_m to k_{ac} at P18 is greater than at P11 (Fig. 12c). This suggests that the influence of active carbons is more important father downstream, because the adsorption time of active carbons would be longer (Fig.5).

C_m appears to be less sensitive to changes of k_{ac} compared with the sensitivity induced by u and D (Fig. 12d for P11). This suggests that the adsorption coefficient of active carbons has less effect on the peak concentration than those of u and D. For L_m, u is much more influential than D and k_{ac} (Fig. 12e). Thus the control of flow rate can be an effective way to manage the spatial extent of pollution. Comparison of the sensitivities of T_m to u, D and k_{ac} shows that the effect of u on T_m is slightly greater than those of other two factors (Fig. 12d). Thus measures based on manipulating u, D and k_{ac} can all be effective options for managing the temporal range of pollution.

4 Concluding remarks

Based on analyses of the monitoring data collected during a major benzene pollution incident on the Huaihe River with assistance of a mathematical model, this study examined the processes and critical conditions underlying the emergency measures implemented to mitigate the impact of the incident. The flow reduction slows down the transport of benzene downstream, allowing more time for benzene dilution via mixing with ambient water and attenuation through reactions. The in-situ treatment using AC absorption removes benzene from the river water. The combination of both measures in dealing with the actual incident was proved to be very effective.

The developed mathematical model was demonstrated to be capable of simulating the benzene transport and transformation in the river. The results showed that volatilization and AC-adsorption dominated the removal of benzene from the river water. To deal with a pollution incident with accidental release of contaminants, this model can be used as a tool to predict the pollution extent (as shown in Fig. 9) under different emergency management scenarios and assess the effectiveness of different measures that can be implemented to mitigate the impact of the incident.

However, the model coefficients were assumed to be constants in the river segments. In reality, these coefficients may vary considerably with time and distance. Therefore, further model development in the future can focus on how to incorporate further temporal and spatial variations of the river systems. In this study, no consideration was given to the fate of activated carbons with a large amount of benzene adsorbed. Would the carbon particles enter the streambed and affect the eco-system of the hyporheic zone? Would the adsorbed benzene become mobile and get released to the river water? Moreover, how should the secondary pollution be considered in dealing with a major pollution incident using an in-situ treatment method that only removes the pollutant from the river water (temporarily) but not completely from the river system? These questions will provide directions for future research as motivated by the present study.

Acknowledgments

This research has been supported by the Natural Science Foundation of China (51421006, 51679065), the Basic Research Programs (Natural Science Foundation) of Jiangsu Province (BK20171436), Social Development - Major Demonstration of Science and Technology of Science and Technology Projects of Jiangsu Province (BE2018737), and the 111 Project (B17015), Ministry of Education and State Administration of Foreign Experts Affairs, P. R. China.

References

Beng, P. (2010). The research and application of the Hydrodynamic mathematical model on the middle part of the Huai River between Bengbu

Gate to Laozishan. (Doctoral dissertation, Hefei University of Technology).

Bjerg, P. L., Sonne, A. T., Rasmussen, J. J., Höss, S., Rønde, V., Traunspurger, W., & McKnight, U. S. (2017). Assessment of groundwater contamination impacting stream ecosystems. In 14th International Conference Sustainable Use and Management of Soil, Sediment and Water Resources (AquaConSoil).

Bjerklie, D. M., Dingman, S. L., & Bolster, C. H. (2005). Comparison of constitutive flow resistance equations based on the Manning and Chezy equations applied to natural rivers. Water resources research, 41(11).

Deng, Z. Q., Bengtsson, L., Singh, V. P., & Adrian, D. D. (2002). Longitudinal dispersion coefficient in single-channel streams. Journal of Hydraulic Engineering, 128(10), 901-916.

Duan, W., He, B., Takara, K., Luo, P., Nover, D., Sahu, N., & Yamashiki, Y. (2013). Spatiotemporal evaluation of water quality incidents in Japan between 1996 and 2007. Chemosphere, 93(6), 946-953.

Feijoó, C., Messetta, M. L., Hegoburu, C., Vázquez, A. G., Guerra-López, J., Mas-Pla, J & Butturini, A. (2018). Retention and release of nutrients and dissolved organic carbon in a nutrient-rich stream: A mass balance approach. Journal of Hydrology, 566, 795-806.

Fischer, H. B. (1975). Discussion of 'simple method for predicting dispersion in streams' by RS McQuivey and TN Keefer. J. Environ. Eng, 504(101), 3.

Fu, W., Fu, H., Skøtt, K., & Yang, M. (2008). Modeling the spill in the Songhua River after the explosion in the petrochemical plant in Jilin. Environmental Science and Pollution Research, 15(3), 178.

Ji, L., Liu, J., Li, Z., Pan, B., & Sun, M. (2017). Accidents of Water Pollution in China in 2011-2015 and Their Causes. Journal of Ecology and Rural Environment, 33(9), 775-782. DOI:10.11934/j.issn.1673-4831.2017.09.002.

Jin, G., Jiang, Q., Tang, H., Li, L., & Barry, D. A. (2018). Density effects on nanoparticle transport in the hyporheic zone. Advances in Water Resources, 121, 406-418.

Jin, G., Zhang, Z., Tang, H., Xiaoquan, Y., Li, L., & Barry, D. A. (2019). Colloid transport and distribution in the hyporheic zone. Hydrological Processes, 33(6), 932-944.

Kumar, A., Jaiswal, D. K., & Kumar, N. (2009). Analytical solutions of one-dimensional advection-diffusion equation with variable coefficients in a finite domain. Journal of Earth System Science, 118(5), 539-549.

Mandaric, L., Kalogianni, E., Skoulikidis, N., Petrovic, M., & Sabater, S. (2019). Contamination patterns and attenuation of pharmaceuticals in a temporary Mediterranean river. Science of the total environment, 647, 561-569.

Majumder, P. S., & Gupta, S. K. (2003). Hybrid reactor for priority pollutant nitrobenzene removal. Water research, 37(18), 4331-4336.

Palumbo-Roe, B., Banks, V. J., Bonsor, H. C., Hamilton, E. M., & Watts, M. J. (2017). Limitations on the role of the hyporheic zone in chromium natural attenuation in a contaminated urban stream. Applied geochemistry, 83, 108-120.

Ren, J., & Packman, A. I. (2005). Coupled Stream− Subsurface Exchange of Colloidal Hematite and Dissolved Zinc, Copper, and Phosphate. Environmental science & technology, 39(17), 6387-6394.

Roy, J. W., Grapentine, L., & Bickerton, G. (2018). Ecological effects from groundwater contaminated by volatile organic compounds on an urban stream's benthic ecosystem. Limnologica, 68, 115-129.

Saup, C. M., Williams, K. H., Rodríguez-Freire, L., Cerrato, J. M., Johnston, M. D., & Wilkins, M. J. (2017). Anoxia stimulates microbially catalyzed metal release from Animas River sediments. Environmental Science: Processes & Impacts, 19(4), 578-585.

Tiseo, I. (2018). Number of serious water pollution incidents in the United Kingdom (UK) from 2001 to 2016, by category. Statista. https://www.statista.com/statistics/820359/serious-water-pollution-incidents-united-kingdom-uk/

Trapp, S., & Harland, B. (1995). Field test of volatilization models. Environmental Science and Pollution Research, 2(3), 164-169.

Van Genuchten, M. T. (1982). Analytical solutions of the one-dimensional convective-dispersive solute transport equation (No. 1661). US Department of Agriculture, Agricultural Research Service.

Wang, C., & Ongley, E. D. (2004). Transjurisdictional water pollution management: The Huai River example. Water international, 29(3), 290-298.

Wang, C., Wang, Y. Y., & Wang, P. F. (2006). Water quality modeling and pollution control for the Eastern route of South to North water transfer project in China. Journal of Hydrodynamics, 18(3), 253-261.

Wang, S., Hu, X., & Chu, D. (2014). Analysis of the river roughness of Huaihe River channels in lower reaches of Bengbu before and after its regulation. Advances in Science and Technology of Water Resources, 34(6), 62-65.

Zhao, J. S., & Ward, O. P. (1999). Microbial degradation of nitrobenzene and mono-nitrophenol by bacteria enriched from municipal activated sludge. Canadian journal of microbiology, 45(5), 427-432.

Zuo, Q., Chen, H., Dou, M., Zhang, Y., & Li, D. (2015). Experimental analysis of the impact of sluice regulation on water quality in the highly polluted Huai River Basin, China. Environmental monitoring and assessment, 187(7), 450.

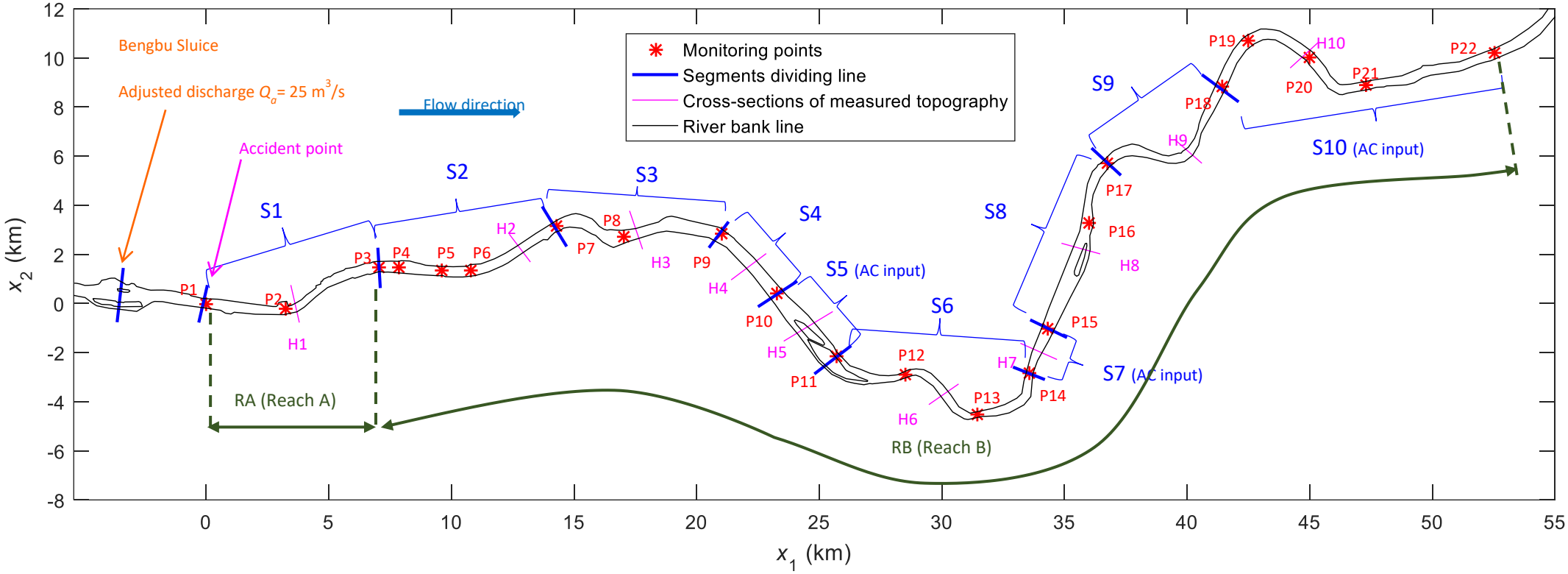

Fig. 1 Map of the studied section of the Huaihe River with highlights of the accident point, 22 monitoring stations (P1-P22), 10 segment divisions (S1-S10), 10 cross-sections measured (H1-H10) and three AC input locations.

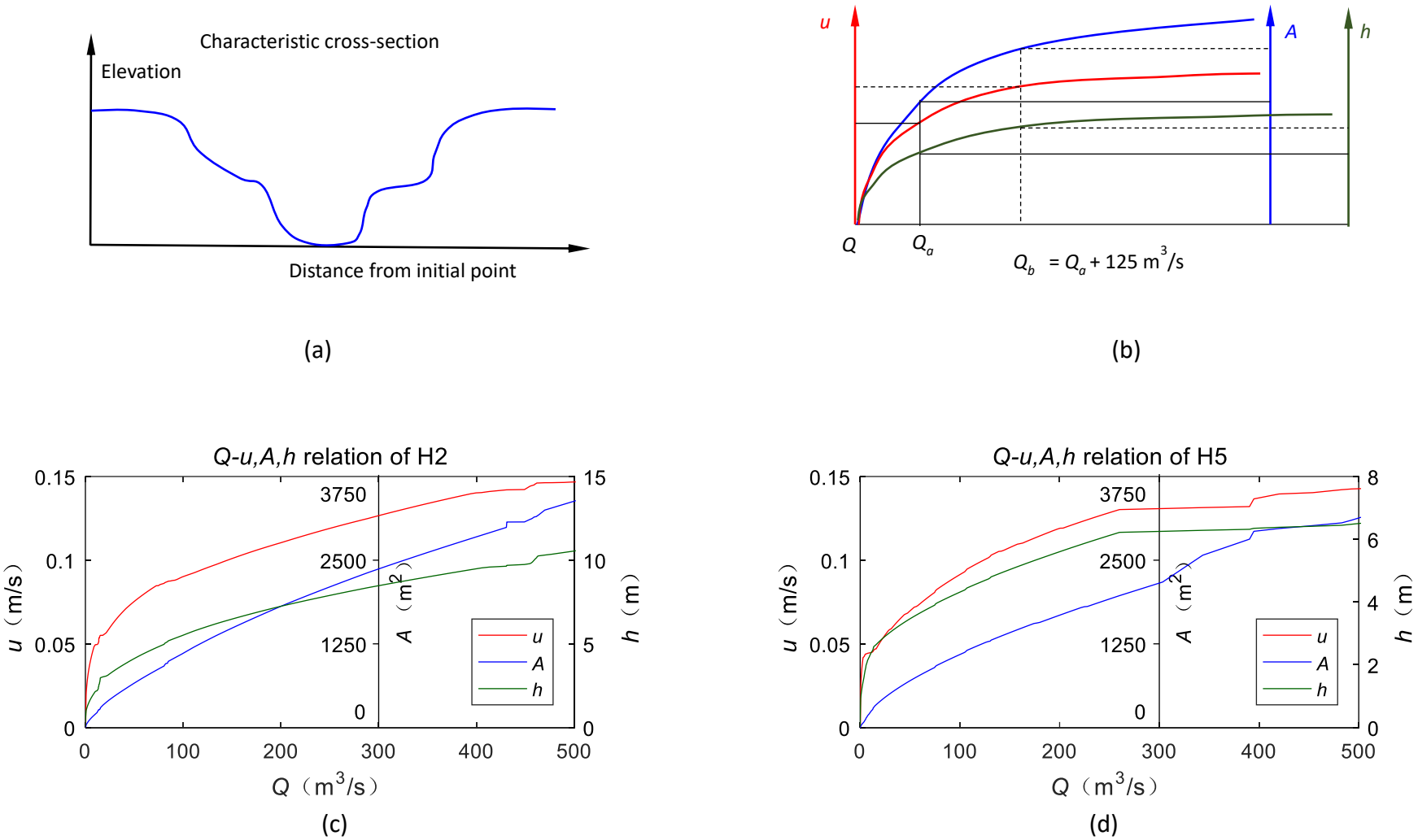

Fig.2 (a) Typical geometry of the river cross-section. (b) Relationships among discharge, average flow velocity, area of cross-section and average depth. (c) and (d) are for H2 and H5, respectively.

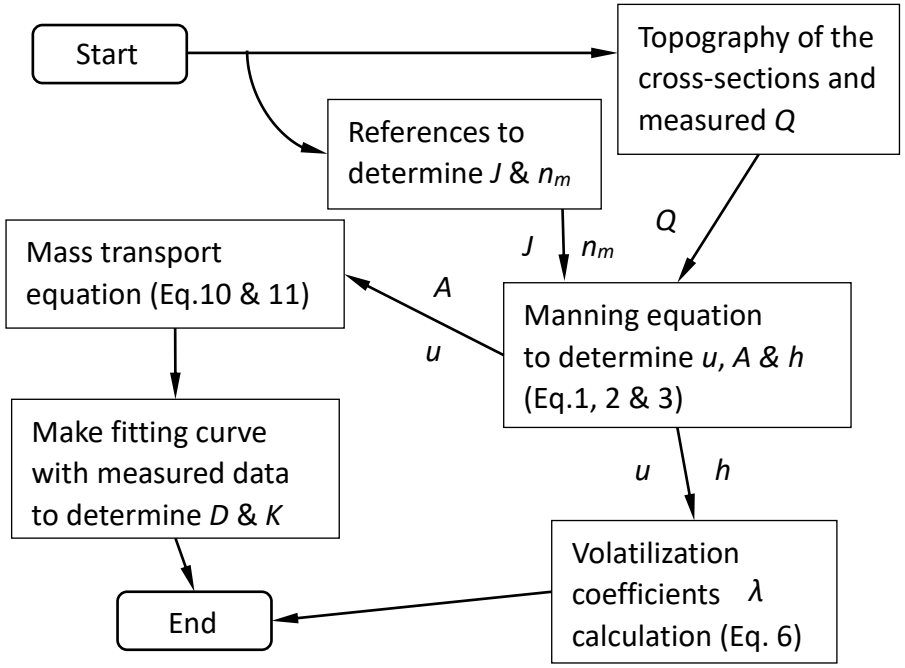

(a)

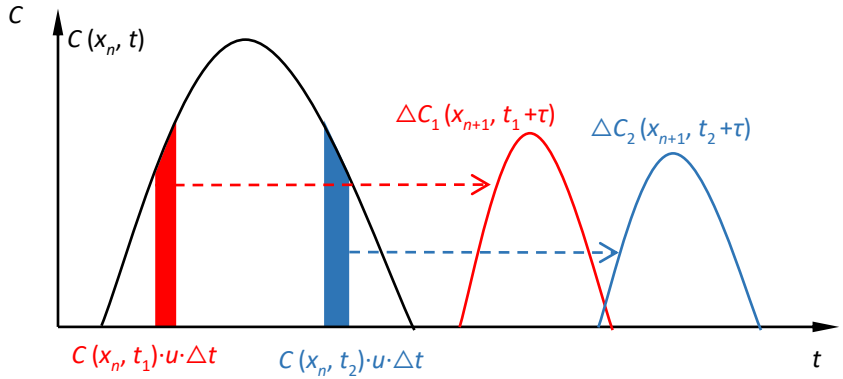

(b)

Fig. 3 (a) Flow-process diagram for the simulation. (b) Transport of benzene downstream (illustration for the derivation of equation (10).

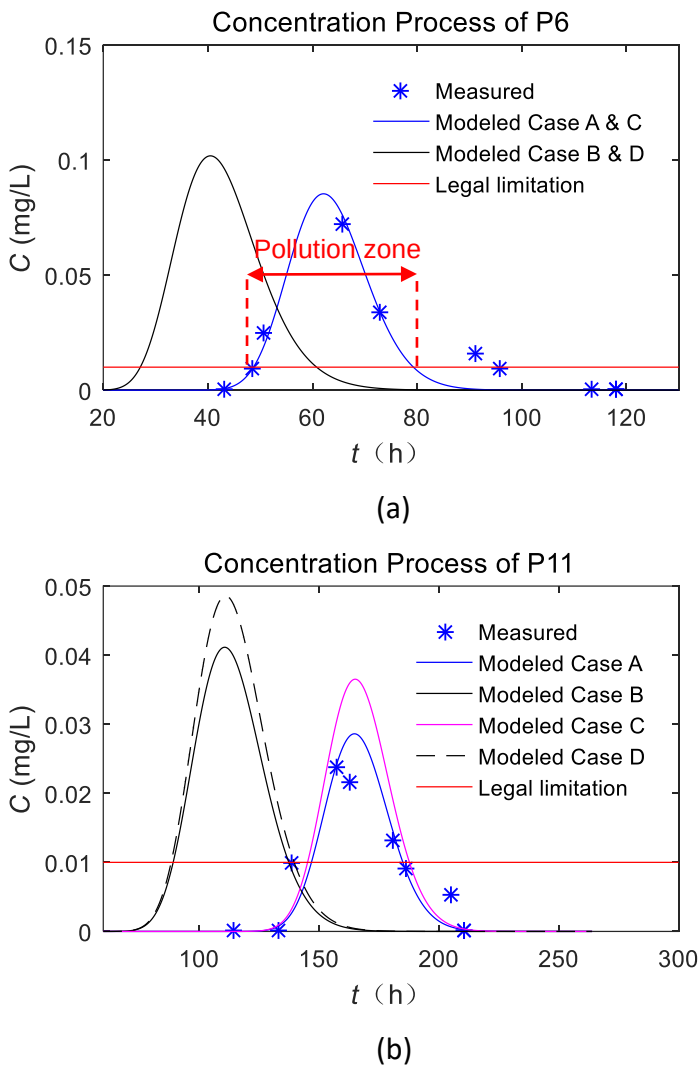

Fig. 4 Comparison of measured and modeled benzene concentrations in the river water at P6 (a) and P11 (b). AC had not been put in P6, but in P11. The red line indicates the regulatory limit of benzene concentration in the river water.

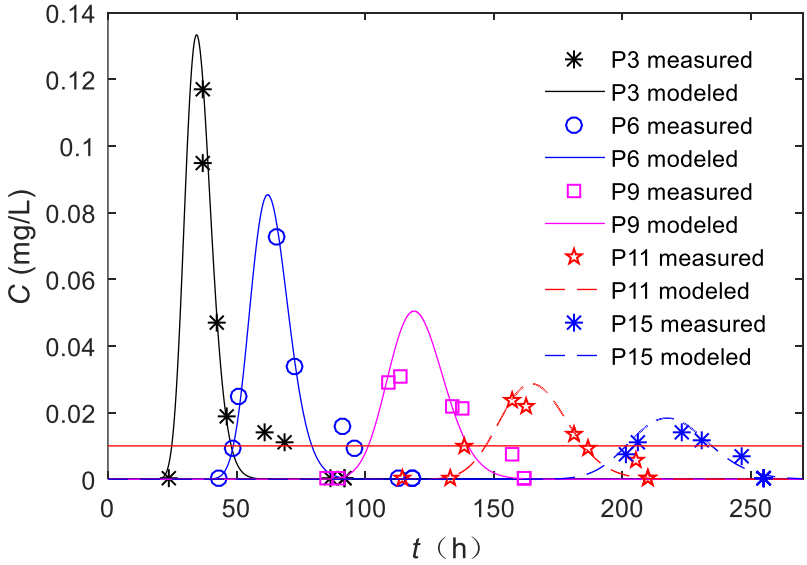

Fig. 5 Comparison of measured and modeled benzene concentrations at different monitoring locations. The red line indicates the regulatory limit of benzene concentration in the river water.

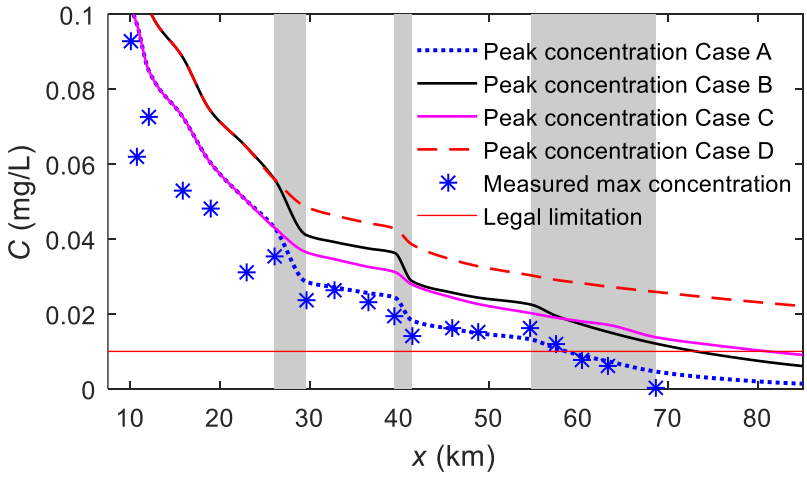

Fig. 6 Comparison of measured and modeled peak concentrations varying with distance. The grey belts show segments of AC input. The red line indicates the regulatory limit of benzene concentration in the river water. The peak concentrations drop sharply where AC are input.

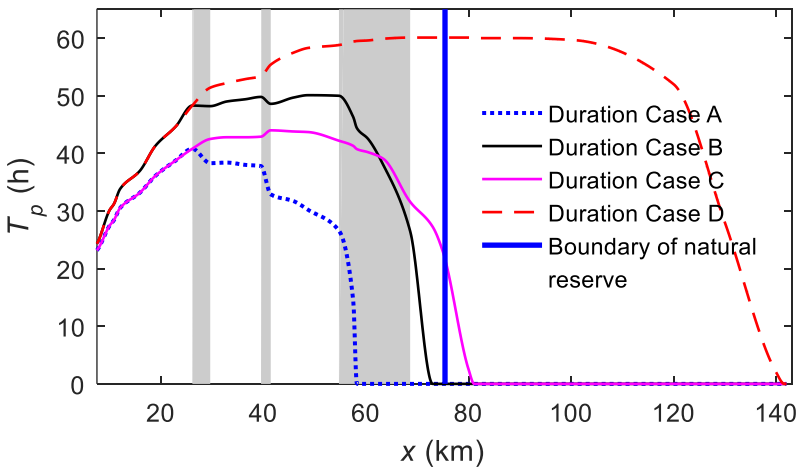

Fig. 7 Pollution duration at different locations for each case. The grey belts show segments of AC input. The durations drop sharply where AC are input.

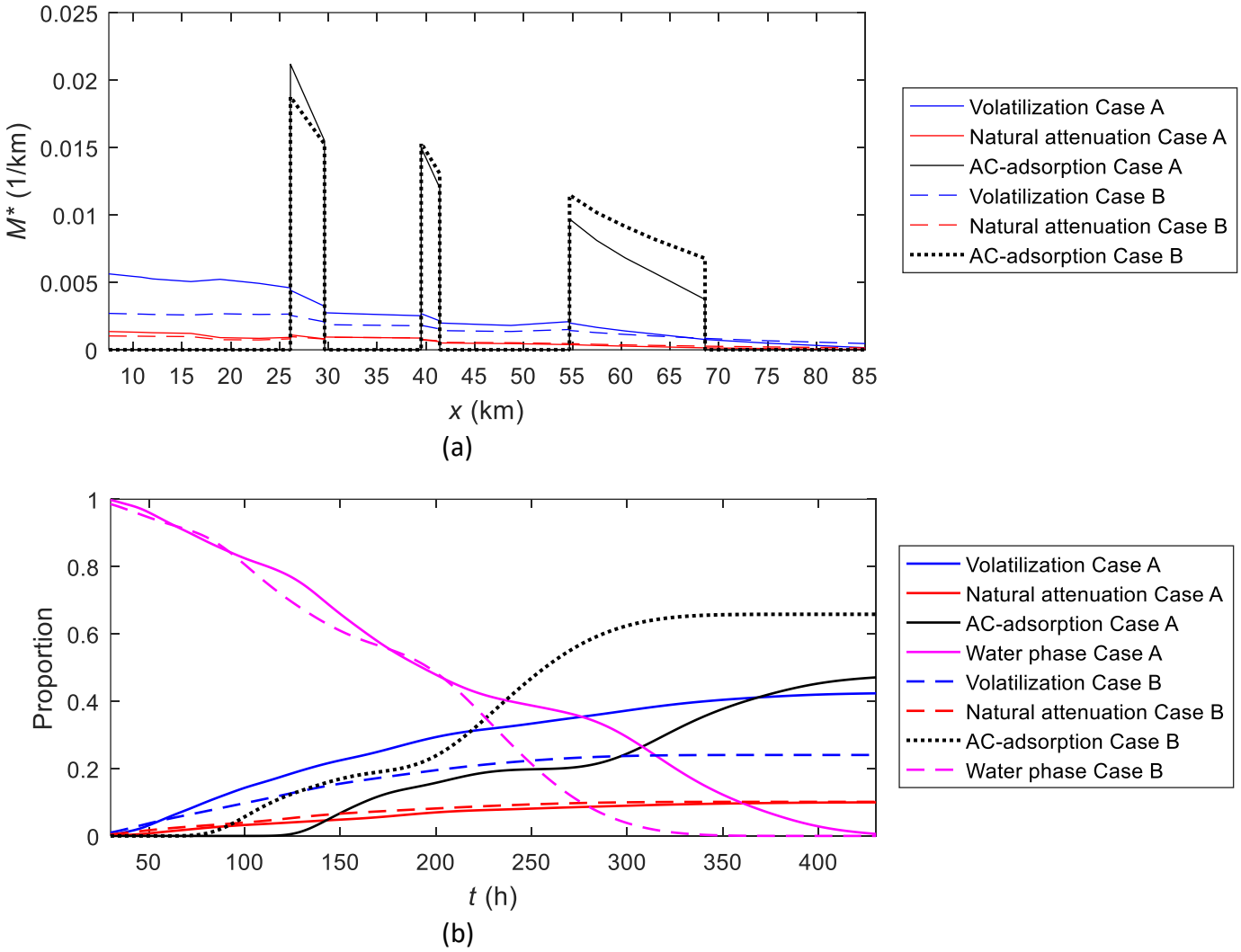

Fig. 8 (a) Normalized benzene mass in each phase varying with distance. The AC-adsorbed phase is suddenly much higher at the segments where the AC are input. (b) Proportions of benzene in each phase over the whole river section varying with time. The AC-adsorbed phase is increasing dramatically when the peak pollution reaches the segments where AC are input.

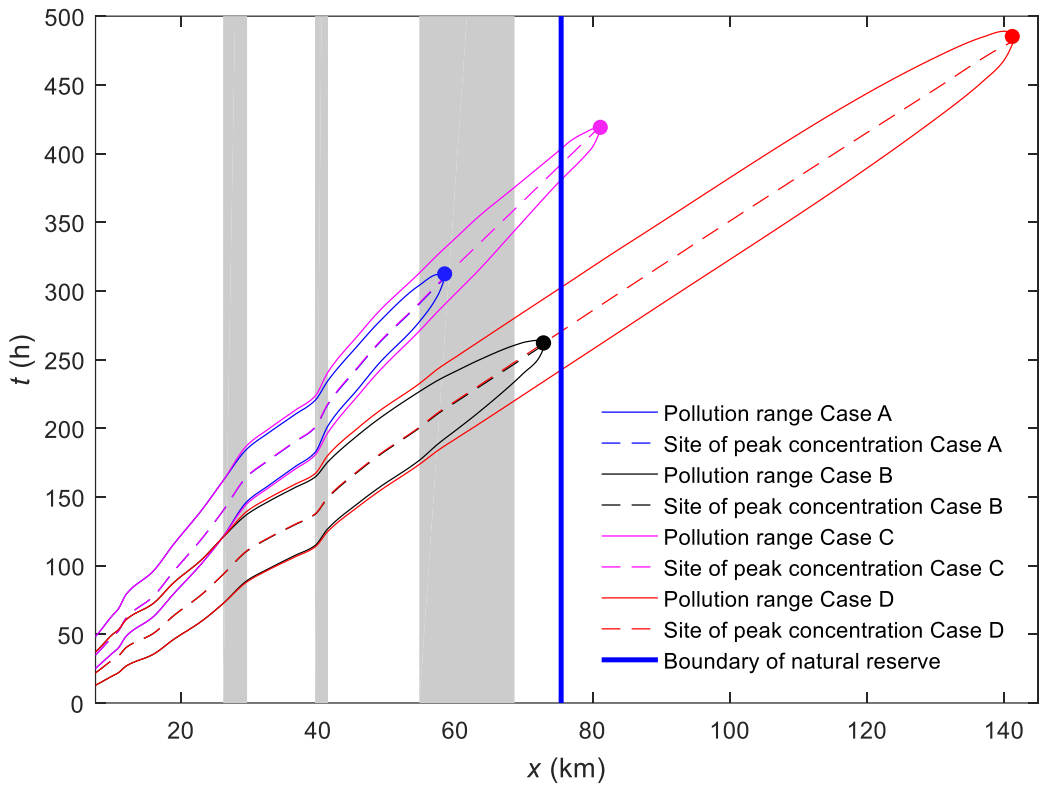

Fig. 9 Spatial and temporal extent of the pollution zone for Case A, B, C & D. The grey belts show segments of AC input. The dashed lines present the spatial and temporal arrival of the peak concentration. The thick blue line represents the upstream boundary of the natural reserve.

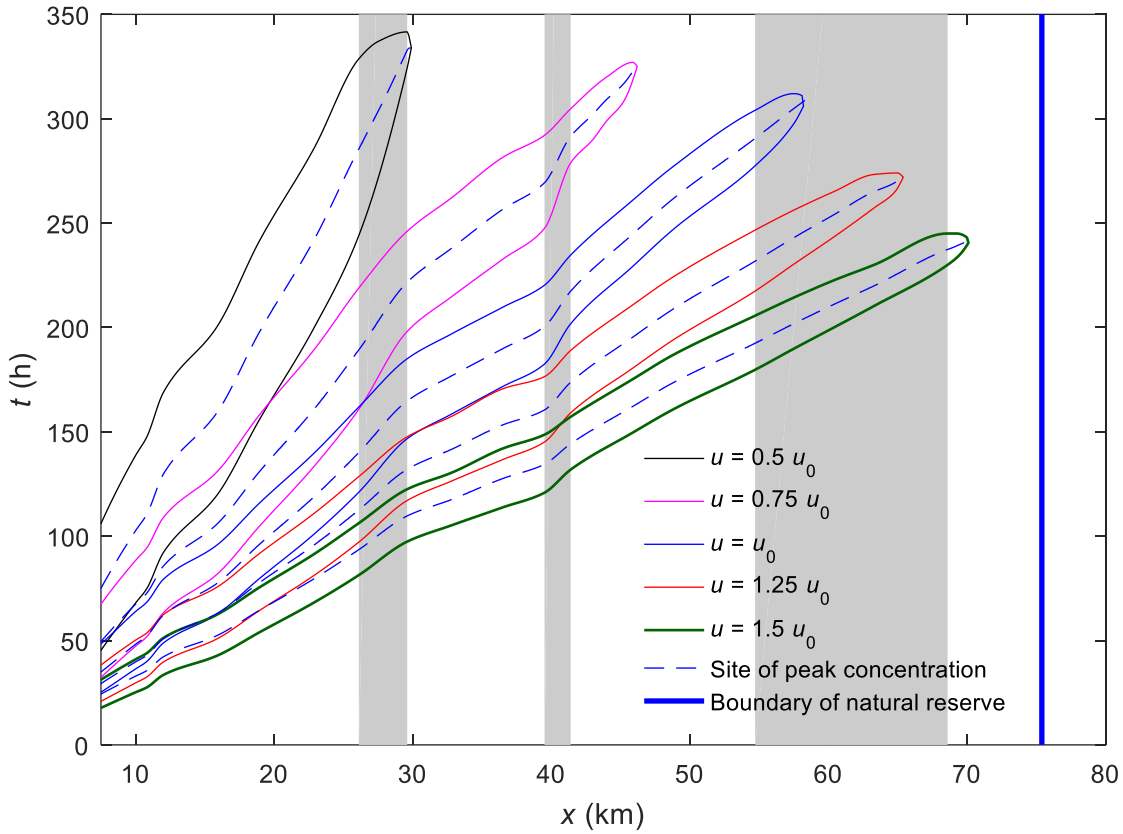
350
300
250
200
150
100
50
0
t (h)
10
20
30
40
50
60
70
80
x (km)
u = 0.5 u0
u = 0.75 u0
u = u0
u = 1.25 u0
u = 1.5 u0
Site of peak concentration
Boundary of natural reserve

(a)

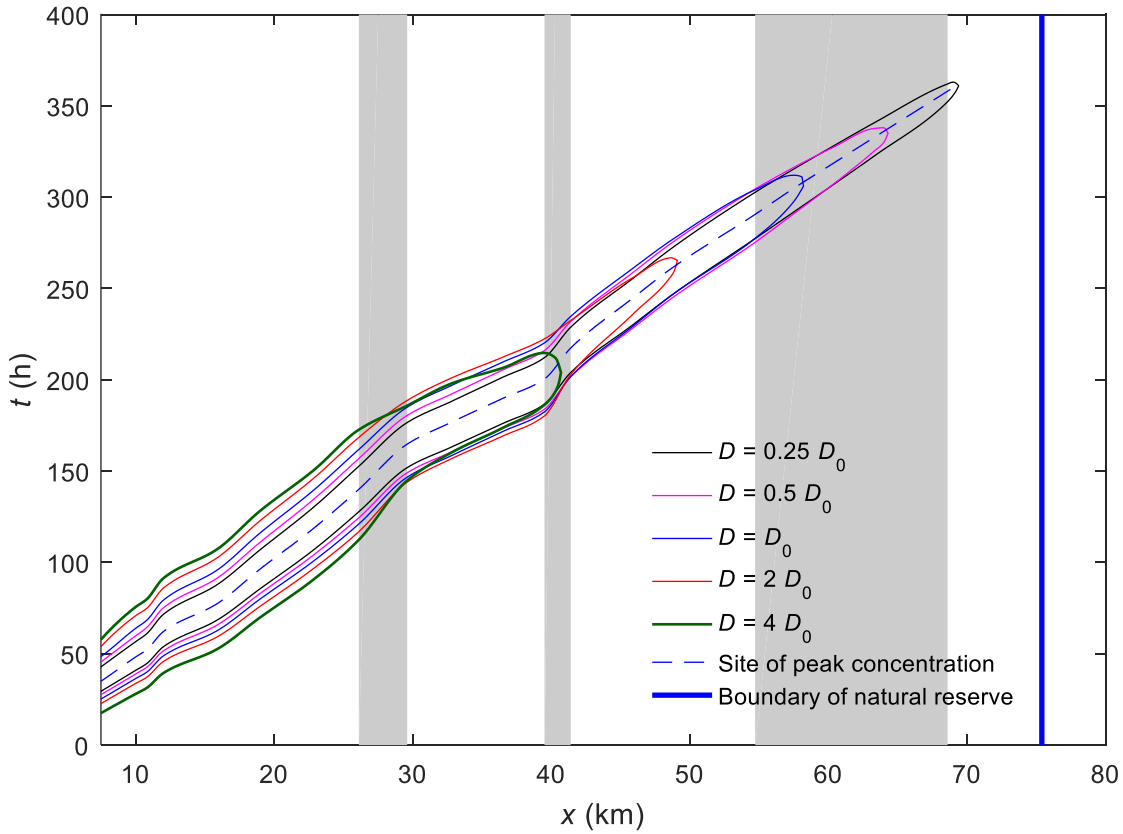
400
350
300
250
200
150
100
50
0
t (h)
10
20
30
40
50
60
70
80
x (km)
D = 0.25 D0
D = 0.5 D0
D = D0
D = 2 D0
D = 4 D0
Site of peak concentration
Boundary of natural reserve

(b)

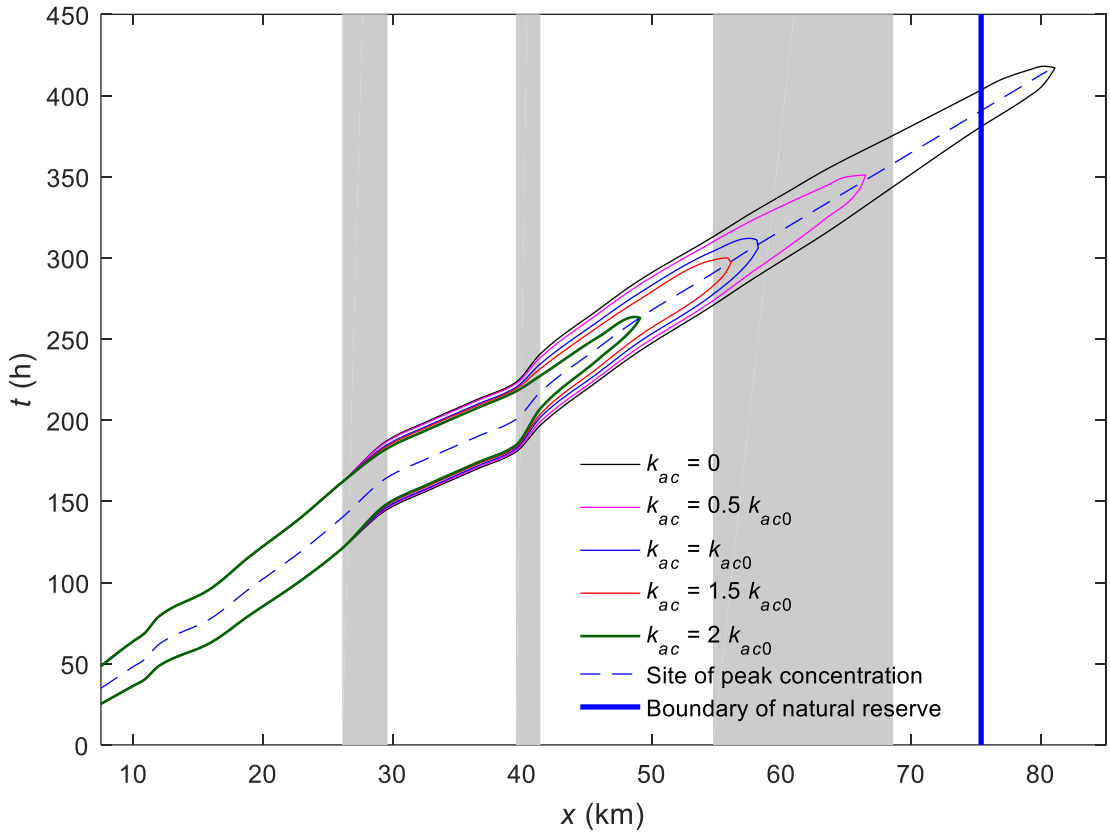

(c)

Fig. 10 Spatial and temporal extent of the pollution zone for cases with different parameters. The grey belts show segments of AC input. The dashed lines present the spatial and temporal arrival of the peak concentration. The thick blue line represents the upstream boundary of the natural reserve. (a) With different flow rates (u). (b) With different dispersion coefficients (D). (c) With different adsorption coefficients of activated carbons (k_{ac}). The arrival times of peak concentration are overlapped for (b) and (c).

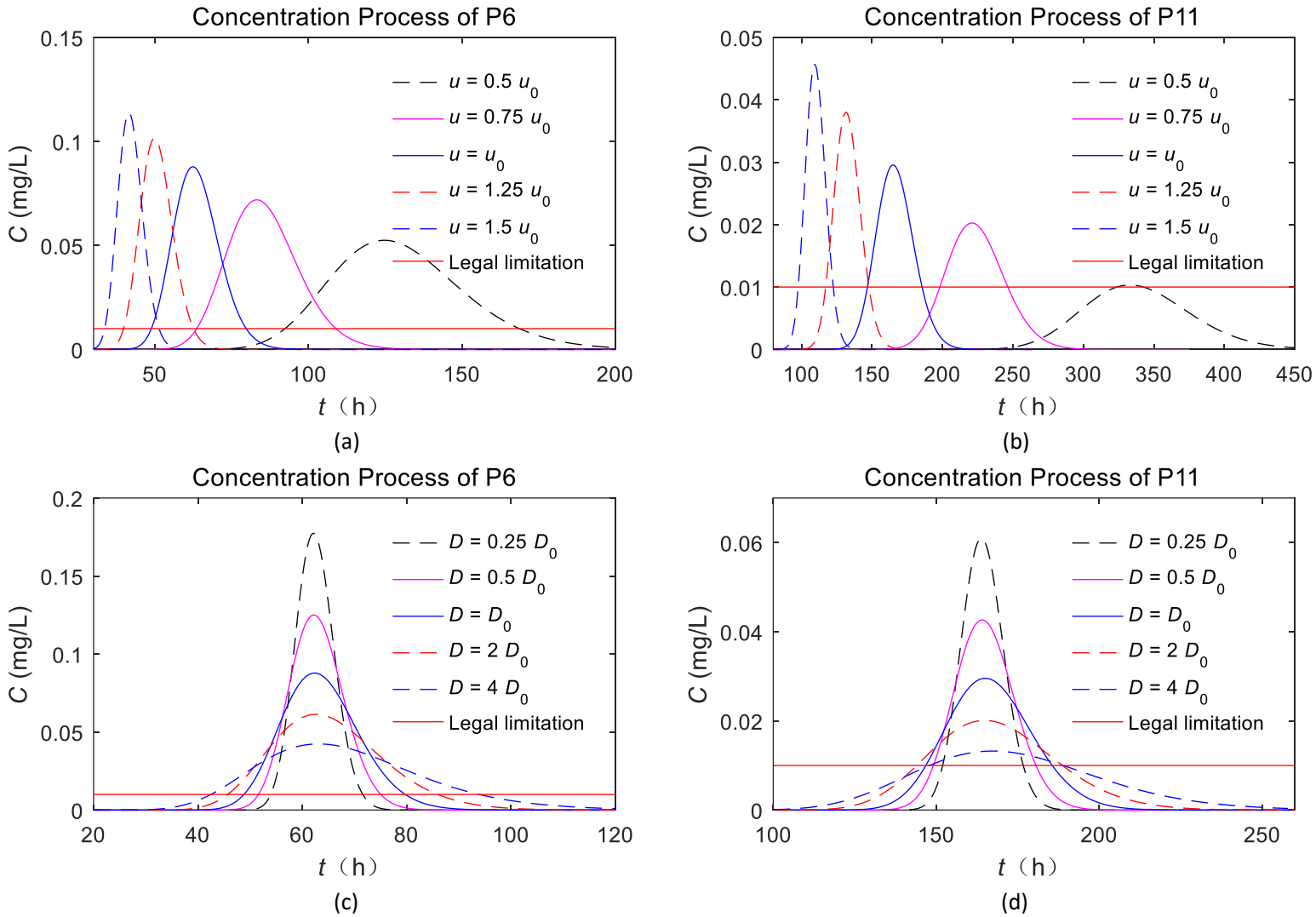
Concentration Process of P6
C (mg/L)
t（h）
u = 0.5 u0
u = 0.75 u0
u = u0
u = 1.25 u0
u = 1.5 u0
Legal limitation
(a)
Concentration Process of P11
C (mg/L)
t（h）
u = 0.5 u0
u = 0.75 u0
u = u0
u = 1.25 u0
u = 1.5 u0
Legal limitation
(b)
Concentration Process of P6
C (mg/L)
t（h）
D = 0.25 D0
D = 0.5 D0
D = D0
D = 2 D0
D = 4 D0
Legal limitation
(c)
Concentration Process of P11
C (mg/L)
t（h）
D = 0.25 D0
D = 0.5 D0
D = D0
D = 2 D0
D = 4 D0
Legal limitation
(d)

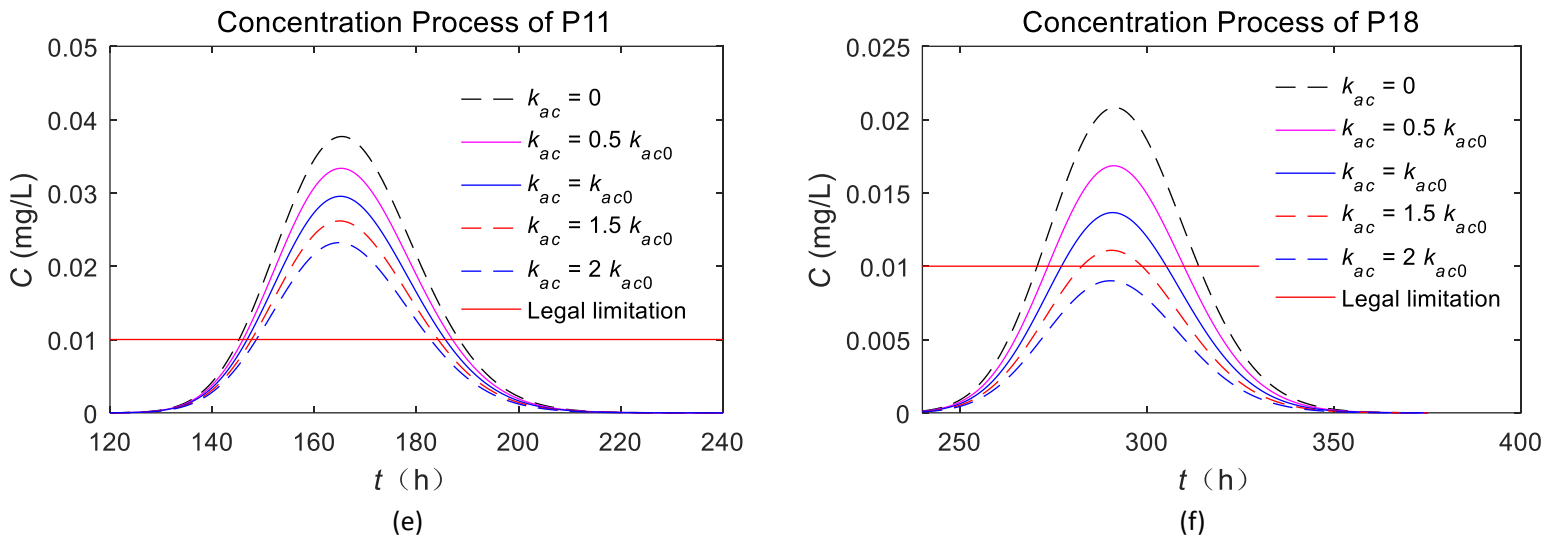

Fig. 11 Comparison of benzene concentrations with different flow rates (u) at P6 (a) and P11 (b), with different dispersion coefficients (D) at P6 (c) and P11 (d), and with different adsorption coefficients of activated carbons (k_{ac}) at P11 (e) and P18 (f). The red line indicates the regulatory limit of benzene concentration in the river water.

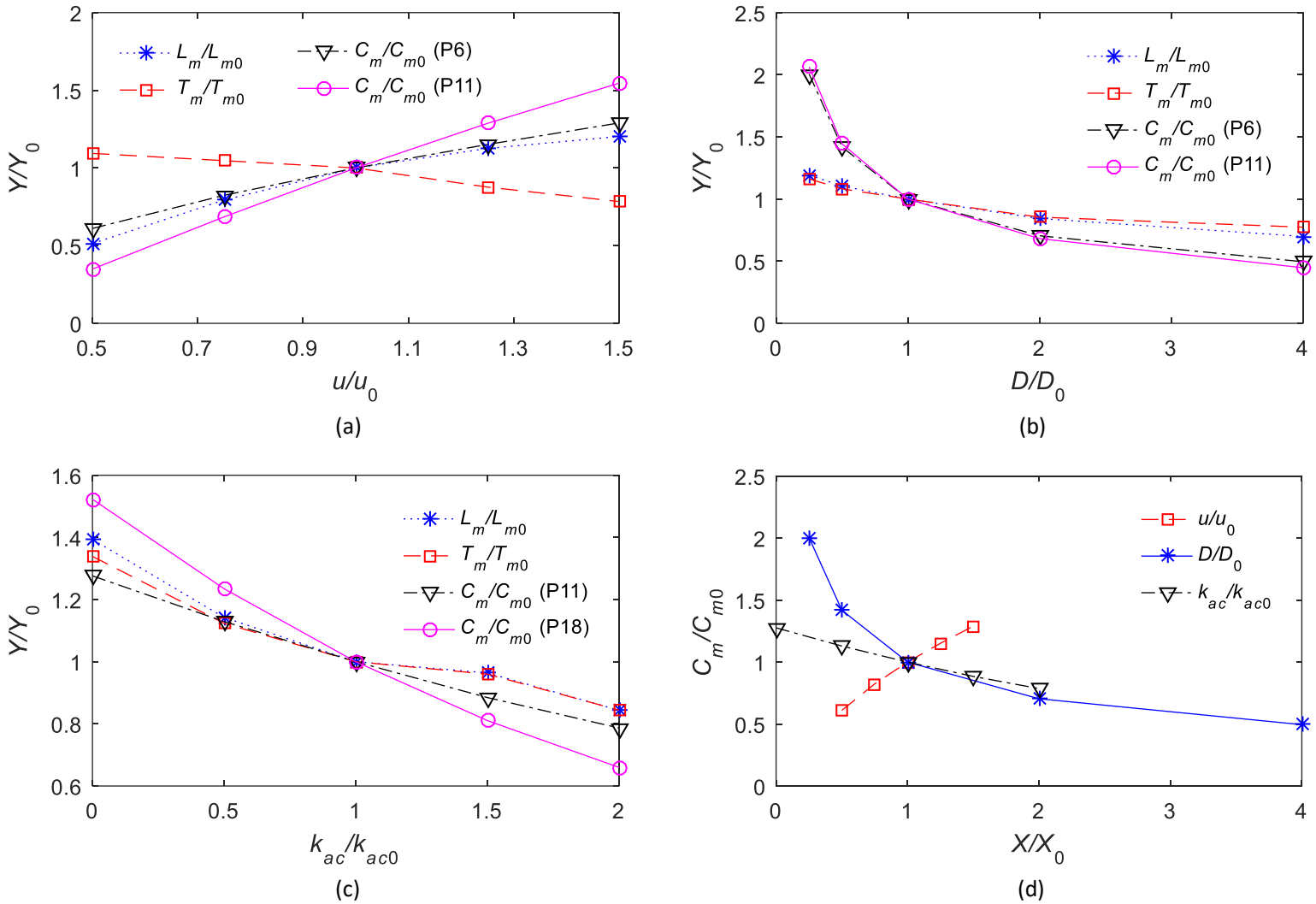
L_m/L_{m0}
T_m/T_{m0}
C_m/C_{m0} (P6)
C_m/C_{m0} (P11)
Y/Y_0
u/u_0
(a)
L_m/L_{m0}
T_m/T_{m0}
C_m/C_{m0} (P6)
C_m/C_{m0} (P11)
Y/Y_0
D/D_0
(b)
L_m/L_{m0}
T_m/T_{m0}
C_m/C_{m0} (P11)
C_m/C_{m0} (P18)
Y/Y_0
k_{ac}/k_{ac0}
(c)
u/u_0
D/D_0
k_{ac}/k_{ac0}
C_m/C_{m0}
X/X_0
(d)

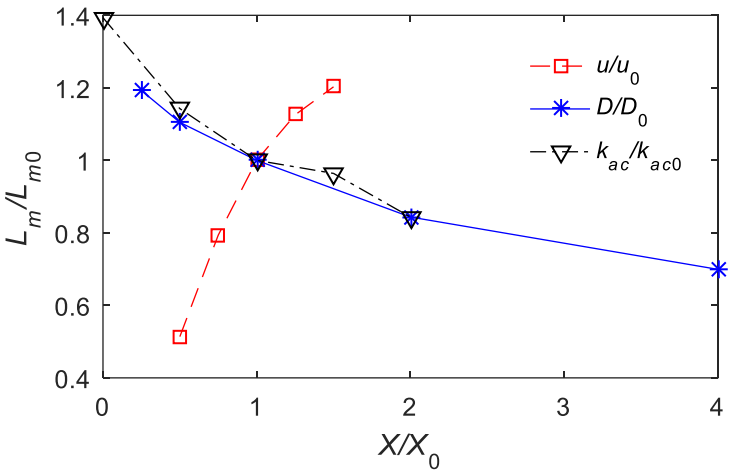

(e)

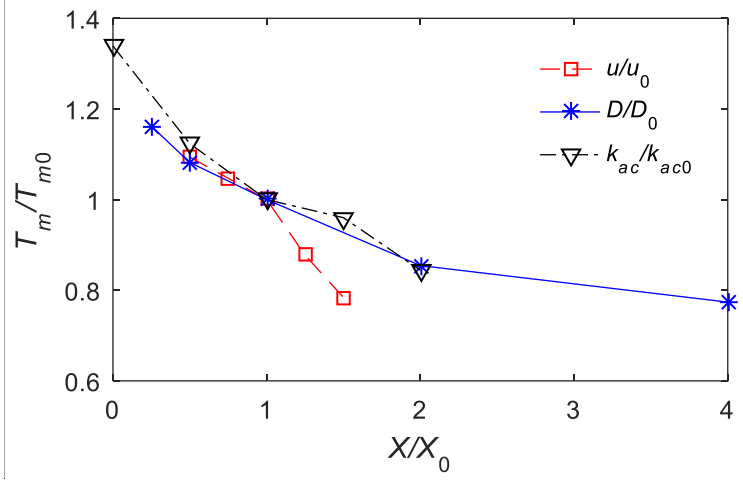

(f)

Fig.12 Sensitives of different parameters. *Y* can represent the pollution length (L_m), pollution duration (T_m), and peak concentration (C_m). *X* can represent dispersion coefficients (*D*), flow rates (*u*), and adsorption coefficients of activated carbons (k_{ac}). (a) The sensitivity of *u* to *Y*. (b) The sensitivity of *D* to *Y*. (c) The sensitivity of k_{ac} to *Y*. (d) The sensitivity of *X* to C_m at P11. (e) The sensitivity of *X* to L_m. (f) The sensitivity of *X* to T_m.

Table 1 Coefficients combination.

Points	x (km)	R	Segment	L (km)	AC input	λ (1/s) Case A & C	λ (1/s) Case B & D	k_{na} (1/s)	k_{ac} (1/s) Case A & B	D (m^2/s)
P1	0.0	/	S1							
P2	3.2	/	S1	7.4	No	2.17×10^{-5}	2.17×10^{-5}	1.34×10^{-7}	0	4.62
P3	7.4	0.9837	S1							
P4	8.2	0.9796	S2							
P5	10.8	0.9524	S2	8.5	No	5.58×10^{-7}	2.95×10^{-7}	1.34×10^{-7}	0	5.66
P6	12.0	0.9637	S2							
P7	15.9	0.9252	S2							
P8	18.9	0.9467	S3	7.0	No	6.04×10^{-7}	3.10×10^{-7}	1.04×10^{-7}	0	4.52
P9	22.9	0.9232	S3							
P10	26.1	0.9733	S4	3.2	No	5.95×10^{-7}	3.22×10^{-7}	1.19×10^{-7}	0	4.38
P11	29.6	0.9534	S5	3.5	Yes	5.71×10^{-7}	3.11×10^{-7}	1.43×10^{-7}	2.74×10^{-6}	3.52
P12	32.8	0.9743	S6							
P13	36.5	0.9669	S6	9.9	No	4.86×10^{-7}	2.79×10^{-7}	1.67×10^{-7}	0	8.42
P14	39.5	0.9860	S6							
P15	41.4	0.9528	S7	1.9	Yes	5.15×10^{-7}	2.84×10^{-7}	1.45×10^{-7}	2.88×10^{-6}	3.19
P16	45.9	0.8472	S8	7.3	No	4.76×10^{-7}	2.62×10^{-7}	1.22×10^{-7}	0	5.42
P17	48.7	0.7162	S8							
P18	54.7	0.6247	S9	6.0	No	5.94×10^{-7}	3.01×10^{-7}	1.10×10^{-7}	0	5.25
P19	57.5	0.5595	S10							
P20	60.4	0.8534	S10	13.9	Yes	5.65×10^{-7}	2.86×10^{-7}	1.10×10^{-7}	2.75×10^{-6}	5.84
P21	63.3	0.9426	S10							
P22	68.6	/	S10							

Table 2 Distributions of benzene in the three different cases at RB

Case	Volatilized	Naturally attenuated	AC-adsorbed
Case A	42.44%	9.99%	47.57%
Case B	24.04%	10.13%	65.83%
Case C	81.14%	18.86%	0.00%
Case D	70.55%	29.45%	0.00%

Table 3 Four simulation cases and simulated spatial and temporal extents of pollution

Cases	Conditions	Spatial and temporal range	
		Duration (T_m, h)	Length (L_m, km)
Case A*	Adjustment; AC input (real)	312.5	58.2
Case B	No adjustment; AC input	264.4	73.0
Case C	Adjustment; No AC input	418.4	81.1#
Case D	No adjustment; No AC input	489.3	141.6#

* Case A represents the real condition.

Downstream of the natural reserve, indicating damages on the reserve.

Table 4 Simulated spatial and temporal extents of pollution for different parameters.

Cases	Conditions	Spatial and temporal range	
		Duration (T_m, h)	Length (L_m, km)
Case U1	$u = 0.5\ u_0$	341.8	29.9
Case U2	$u = 0.75\ u_0$	327.2	46.2
Case U3*	$u = u_0$	312.5	58.2
Case U4	$u = 1.25\ u_0$	274.1	65.5
Case U5	$u = 1.5\ u_0$	245.0	70.0
Case D1	$D = 0.25\ D_0$	363.1	69.4
Case D2	$D = 0.5\ D_0$	338.1	64.3
Case D3*	$D = D_0$	312.5	58.2
Case D4	$D = 2\ D_0$	267.0	49.1
Case D5	$D = 4\ D_0$	241.8	40.7
Case K1	$k_{ac} = 0$	418.4	81.1#
Case K2	$k_{ac} = 0.5\ k_{ac0}$	351.1	66.5
Case K3*	$k_{ac} = k_{ac0}$	312.5	58.2
Case K4	$k_{ac} = 1.5\ k_{ac0}$	300.0	56.1
Case K5	$k_{ac} = 2\ k_{ac0}$	263.8	49.1

* Represents the real condition.

Downstream of the natural reserve, indicating damages on the reserve.